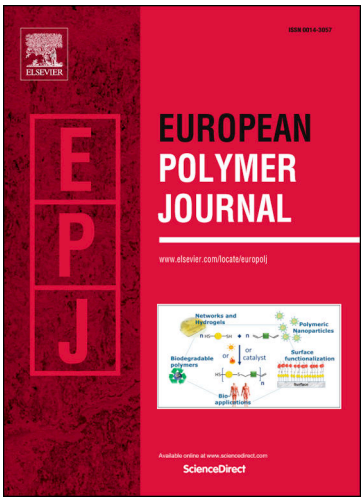

Self-assembly of poly(L-lactide-*co*-glycolide) and magnetic nanoparticles into nanoclusters for controlled drug delivery

Alma Lucia Villela Zumaya, Dominik Martynek, Tereza Bautkinová, Miroslav Šoó š, Pavel Ulbrich, Jean-Marie Raquez, Marcela Dendisová, Jan Merna, Jarmila Vilč áková, Dušan Kopecký, Fatima Hassouna

PII: S0014-3057(20)30452-3
DOI: https://doi.org/10.1016/j.eurpolymj.2020.109795
Reference: EPJ 109795

To appear in: *European Polymer Journal*

Received Date: 25 February 2020
Revised Date: 7 May 2020
Accepted Date: 22 May 2020

Please cite this article as: Lucia Villela Zumaya, A., Martynek, D., Bautkinová, T., Šoó š, M., Ulbrich, P., Raquez, J-M., Dendisová, M., Merna, J., Vilč áková, J., Kopecký, D., Hassouna, F., Self-assembly of poly(L-lactide-*co*-glycolide) and magnetic nanoparticles into nanoclusters for controlled drug delivery, *European Polymer Journal* (2020), doi: https://doi.org/10.1016/j.eurpolymj.2020.109795

Self-assembly of poly(L-lactide-*co*-glycolide) and magnetic nanoparticles into nanoclusters for controlled drug delivery

Alma Lucia Villela Zumaya[1], Dominik Martynek[1], Tereza Bautkinová[1], Miroslav Šoóš[1*], Pavel Ulbrich[3], Jean-Marie Raquez[2], Marcela Dendisová[5], Jan Merna[6], Jarmila Vilčáková[7], Dušan Kopecký[4], Fatima Hassouna[1*]

[1]Department of Chemical Engineering, University Chemistry and Technology, Prague, Technická 5, 166 28 Prague 6, Czech Republic

[2]Laboratory of Polymeric and Composite Materials, University of Mons (UMONS), Place du Parc 20, 7000 Mons, Belgium

[3]Department of Biochemistry and Microbiology, University of Chemistry and Technology Prague, Technická 5, 166 28 Prague 6, Czech Republic

[4]Department of Computing and Control Engineering, University of Chemistry and Technology Prague, Technická 5, 166 28 Prague 6, Czech Republic

[5]Department of Physical Chemistry, University of Chemistry and Technology Prague, Technická 5, 166 28 Prague 6, Czech Republic

[6]Department of Polymers, University of Chemistry and Technology Prague, Technická 5, 166 28 Prague 6, Czech Republic

[7]Centre of Polymer Systems, Tomas Bata University in Zlin, tř. T. Bati 5678, Zlin, 760 01, Czech Republic

Corresponding author:

Assoc. Prof. Fatima Hassouna

Email: fatima.hassouna@vscht.cz

Tel.:+420 220 44 32 23

Prof. Miroslav Šoóš

Email: soosm@vscht.cz

Tel: +420 220 44 32 52

Abstract

The possibility to combine nanoparticles (NPs) with different functionalities into nanoclusters of controlled size and kinetic profile of drug release presents a promising route for the preparation of a multifunctional drug delivery system. In this study, to construct controlled drug delivery (nano)clusters, a simple and versatile method based on self-assembly via electrostatic interactions of oppositely charged poly(lactide-co-glycolide) (PLGA) and superparamagnetic iron oxide (IO) NPs was developed. Drug loaded heteroclusters with controlled size of 224 ± 52 nm and Zeta potential of -51 ± 6 mV were produced. Dissolution tests demonstrated an accelerated drug release in the heteroclusters compared to neat PLGA NPs after 24 h. This was correlated with the catalytic effect of IO NPs on the degradation of PLGA matrix. Moreover, the magnetic properties of the heteroclusters were maintained after the dissolution tests. Hence, even after drug release, the heteroclusters can be used for treatment with magnetically mediated hyperthermia.

Keywords: PLGA nanoparticles; iron oxide nanoparticles; nanoprecipitation; self-assembly; electrostatic interactions; heteroclusters; dissolution tests

1. Introduction

Thanks to the emergence of nanotechnology, enormous steps forward have been done to develop drug delivery systems using NPs as carriers for therapeutic drugs in various diseases, particularly to fight cancer. In fact, even though cancer therapies are being continually improved, there is the reappearance of cancer in the form of metastases in many cases [1, 2]. Numerous methods have been explored, including NPs, liposomes, viral vectors, niosomes, vesicles and capsules [3]. A wide range of particle sizes ranging from 20 to 1000 nm has been reported. Polymeric NPs are being considered as attractive carriers for drug delivery, thanks to their ability to enhance the solubility of poorly water soluble drugs and to extend the drug circulation in the blood stream [4, 5]. In addition, drug polymeric nanocarriers significantly enhance high local concentration of drug at the tumor site, opening the possibility of controlled release of the drug where the therapeutic effect is desired. In this way, the nanocarriers may protect healthy tissues and cells from the drug toxicity, hence minimising any side effects [6, 7]. In order to ensure good biocompatibility and low toxicity, different kind of biocompatible materials have been used to prepare NPs such as poly (lactide) (PLA), poly(lactide-*co*-glycolide) (PLGA), poly (ε-caprolactone) (PCL), chitosan, alginate, gelatin etc. Chemical nature of the polymer and its properties dictate whether it is suitable to host hydrophilic or hydrophobic drugs as well as affects the drug release rate. This is due to the kinetics of polymer degradation induced by hydrolysis or enzymatic degradation. Despite the above-mentioned advances, delivery of a single therapeutic agent is usually insufficient to prevent relapsing of the disease. In this regard, the simultaneous administration of multiple drugs could considerably enhance the success of the treatment. The actual challenge of nanotechnology is presently shifting from the elaboration of individual NPs to their assembly into larger objects in a form of supramolecular systems or nanostructured materials with various functionalities [8, 9].

The advantages of using a multicomponent system include the decrease of cytotoxicity inside the body, the ability to lower the chemotherapeutic drug dose and to improve the pharmacokinetic profiles [10]. Numerous approaches combining several functionalities within single particle have been previously reported [11, 12]. Among them, targeted drug delivery systems with polymers and magnetic NPs have attracted much attention [10, 13]. Magnetic iron oxide NPs (IO NPs) are biocompatible and can be prepared in various sizes [14, 15]. Their magnetic properties permits them to act as contrast agents in magnetic resonance imaging (MRI), they can be used for guided delivery at the location of interest and upon exposure to the magnetic fields they can induce local tissue heating (hyperthermia) [16-18]. This can be applied to trigger the release of a loaded drug and / or to engender cell death (temperature-induced apoptosis) [19]. Despite these advantages, this approach often requires the use of toxic chemicals that can come in contact with the encapsulated biomolecules, thus causing loss of drug bioactivity [20]. In this regard, self-assembly of NPs of various kind and nature, e.g. polymeric and inorganic, into large hierarchical structures will be beneficial to address this issue. Moreover, these NPs can be prepared individually and avoid the usage of toxic chemicals when dealing with biological molecules. Hierarchical structures in the form of clusters composed of NPs of various kind, can be prepared by self-assembly via hydrophobic or electrostatic interactions of oppositely charged entities [21].

In this study, a simple and versatile method based on self-assembly *via* electrostatic interactions of oppositely charged polymeric and inorganic NPs was developed to construct hetero-clusters in a range of nanometres for controlled drug delivery. Owing to its biocompatibility and to its ability to hydrolyse in the body by hydrolytic cleavage of ester bonds, the FDA approved PLGA was used to prepare polymeric NPs loaded with different model drugs by nanoprecipitation [22-24]. IO NPs (i.e. Fe_3O_4) were prepared by co-precipitation method affording flexibility in their surface

functionalization. Different types of FDA approved oppositely charged coatings were applied on the surface of PLGA and IO NPs, particularly alginate (ALG), polyethyleneimine (PEI), chitosan (CHIT) and polyacrylic acid (PAA), to induce NPs self-assembly. Impact of processing conditions such as nature of the coating, ratio between oppositely charged particles and mixing parameters on the size and stability of prepared clusters was evaluated. Furthermore, relationship between the drug release kinetics and NPs/nanoclusters properties (e.g. primary particle size, surface charge, material properties and strength of the interaction) was established.

2. Experimental

2.1. Materials

L-lactide (98%), glycolide (≥99%), polyethyleneimine branched (PEI) (Mw = 25 kDa), sodium alginate, chitosan, iron (III) chloride hexahydrate (≥99%), iron (II) chloride tetrahydrate (98%), polyacrylic acid (Mw= 1800 kDa), potassium dihydrogen phosphate (≥98%), butane-1,4-diol (99%), Tin(II) ethylhexanoate ($Sn(Oct)_2$) (92.5-100.0%), deuterated chloroform (≥99%), and tetramethylsilane (≥99%) were purchased from Sigma-Aldrich. Dialysis bag (Spectra/Por, MWCO: 3.5 kDa) was purchased from ThermoFisher. Commercial PLGA (Purasorb PDLG 7502A, 70/30 LA/GA) was kindly donated by Corbion (Gorinchem, Netherlands). Ibuprofen was kindly donated by Zentiva group (Prague, Czech Republic). Sodium Hydroxide, acetone (p.a 99.5%), dimethyl sulfoxide (DMSO) p.a, ammonia, dichloromethane p.a. and *n*-heptane were purchased from Penta (Prague, Czech Republic). For all experiments, Millipore water was used.

2.2. Synthesis of PLGA by ring opening polymerization

While PLGA can already be used from a commercial supplier, there is a need to control and change the properties of the material, especially for biomedical applications. Therefore, the ability to adjust the molar ratio with the desired molecular weight and properties can be achieved during the

polymerization. For this study, PLGA was synthesized by ring opening polymerization following the procedure described by Erbetta et al. [25] (see Supporting Information). Briefly, the synthesis of PLGA was achieved by polymerization of the monomers L-lactide and glycolide in the presence of catalyst stannous octoate and butane-1,4-diol as co-initiator under nitrogen atmosphere.

2.3. Production of PLGA nanoparticles

Neat as well as drug-loaded PLGA NPs were prepared by nanoprecipitation method [24]. The organic phase containing 50 mg of PLGA, 5 ml acetone and a desired amount of a model drug, i.e. ibuprofen, was stirred using magnetic stirrer until complete dissolution. The ratio of model drug to polymer was set to 1:10 (w/w).The solubility of ibuprofen in acetone is 1.1266 g/ml. Based on the ibuprofen to acetone ratio, the concentration of ibuprofen is 0.001 g/ml, which is well below the solubility limit [27]. Afterwards, the formation of PLGA NPs was induced by dropwise injection of organic solvent containing polymer with a flow rate 0.5 ml/min using a syringe pump (Multi-Phaser TM NE-1010) into 50 ml of the aqueous phase. The aqueous phase containing the required amount of the coating agent, i.e. 0.05 – 0.2 wt. % of PEI for PLGA-PEI and 1 wt. % aqueous solution of ALG for PLGA-ALG was magnetically stirred. In fact, two types of coatings were applied on the surface of PLGA NPs, i.e. ALG and PEI, which provide negative and positive charges on the surface of PLGA NPs, respectively. Concentration of the coating agents has been chosen to avoid any cytotoxic effects [28-30]. Detailed information about the conditions are reported in **Table 1**. The suspension was then left under stirring for 4 hours at room temperature to evaporate the organic solvent. The NPs were purified three times by centrifugation at 14000 rpm for 45 min at 4 °C with deionised water.

Table 1. Experimental conditions used for preparation of polymeric NPs

	Materials	PLGA-PEI 0.05%	PLGA-PEI 0.05%_Ibu	PLGA-PEI 0.2%	PLGA-PEI 0.2%_Ibu	PLGA-ALG 1%
Organic phase	PLGA (mg)	50	50	50	50	50
	Ibuprofen (mg)	-	5	-	5	-
	Acetone (ml)	5	5	5	5	5
Aqueous phase	Polyethyleneimine (PEI) (µg)	25	25	100	100	
	Alginate (ALG) (µg)	-	-	-	-	500
	Millipore water (ml)	50	50	50	50	50

2.4. Synthesis of iron oxide nanoparticles

Three types of Superparamagnetic IO NPs coated with three types of coating agents were prepared by the co-precipitation method [31], i.e. IO-PAA, IO-CHIT and IO-ALG. For preparation of IO-PAA, 0.98 g (4.92 mmol) of iron(II) chloride tetrahydrate and 2.68 g (9.92 mmol) of iron(III) chloride hexahydrate were mixed in the form of water solution for the NPs formation. Both salts were dissolved in a small amount of Millipore water and injected into a round bottom flask with 45 mL of already degassed Millipore water (30 minutes of degassing with nitrogen) then, 3 g of PAA were added to the system. The mixture was heated to 80 °C and subsequently, the dropwise injection of 9.85 mL of ammonium hydroxide led to the formation of a dark suspension. After complete injection, the solution was left under stirring for 30 min. To wash the NPs, the product was precipitated with acetone, decanted with a strong magnet and redispersed in Millipore water. This washing step was repeated one more time. Finally, resulting dispersion of IO NPs was centrifuged at 7000 rpm for 5 min and the supernatant containing a monodisperse population of

particles was collected. The subsequent material was named IO-PAA. The final concentration of IO NPs was about 106 mg/ml.

For the preparation of CHIT and ALG coated IO NPs, no addition of coating agent was employed during the synthesis, while keeping the same procedure. A solution of CHIT was prepared by mixing an acetic acid solution of 0.4 v/v % with CHIT to a final concentration of 2 mg/ml. The chitosan-coated iron oxide (IO-CHIT) NPs were prepared by mixing 5 ml of CHIT solution with 95 µl of uncoated IO NPs suspension and sonicated by ultrasonic probe for 30 min at 40 W with 30 s sonication and 10 s pause in an ice bath. Afterwards, the suspension was washed by centrifugation at 10 000 rpm for 30 min at 4 °C and redispersed in distilled water. In the case of IO-ALG NPs, the same procedure as for IO-CHIT NPs was followed. An alginate solution was prepared by mixing alginate in distilled water for a final concentration of 4 mg/ml. The IO-ALG NPs were prepared by mixing 2.5 ml of ALG solution with 95 µl of IO NPs suspension.

2.5. Formation of clusters

The formation of clusters was based on the electrostatic interactions between the coated polymeric and IO NPs. Two types of clusters were investigated in this work, i.e. homoclusters, composed of same type of NPs while having oppositely charged surfaces, and heteroclusters, composed of different type of NPs while having oppositely charged surfaces. In addition, as the mixing speed of suspensions with oppositely charged NPs can affect the outcome of the process, both one-shot and dropwise addition approaches were considered. The first one involves the addition of the IO or polymeric NPs into the coated polymeric NPs in one single shot. The second approach consists of a slow addition of each suspension, polymeric and IO NPs using a syringe pump (Multi-Phaser TM NE-1010) with fixed flow rate of 0.5 ml/min while dropping it into an empty vial with a magnetic stirrer at 100 rpm. Apart from mixing rate, the impact of ratio between the IO and

polymeric NPs on the final size of formed clusters was also investigated. The ratios of IO and polymeric NPs were considered as the total solid content of the NP suspensions. Solid content was obtained by moisture analyser (Kern and Sohn GmbH Moisture analyser DBS) by dropping 1 ml of suspension in a sand filled aluminum pan. The experimental conditions for homo and heteroclusters preparation are summarized in **Table 2**. For the slow addition approach, the effect of different flow rates for the ratio of 1:1 (w/w) were investigated for both homo and heteroclusters.

Table 2. Experimental conditions used for the formation of the homoclusters and heteroclusters

	PLGA-ALG:PLGA-PEI	**PLGA-ALG 1% (mg)**	**PLGA-PEI 0.05% (mg)**
Homoclusters	1:1	3	3
	1:2	1.5	3
	1:4	0.75	3
	1:6	0.5	3
	1:8	0.375	3
	1:10	0.3	3
	IO-PAA:PLGA-PEI	**IO-PAA (mg)**	**PLGA-PEI 0.05% (mg)**
Heteroclusters	1:1	3	3
	1:2	1.5	3
	1:3	1	3
	1:3.25	0.92	3
	1:3.5	0.86	3
	1:4	0.75	3
	1:5	0.6	3
	1:10	0.3	3
	1:100	0.03	3

2.6. Drug loading and dissolution tests

The drug loading was measured by means of UV-Visible spectrophotometer (Agilent Technology, Cary 60). For measurement, an aliquot of the ibuprofen loaded PLGA suspension was freeze-dried using Freeze Dryer L4-110 PRO (GREGOR Instruments, Czech Republic) at 0.5 hPa for 48 h. The freeze dried sample was dissolved in DMSO for the drug loading measurement. The concentration of ibuprofen in PLGA NPs was measured using a calibration curve constructed from absorbance values of known concentrations of ibuprofen solutions in dimethyl sulfoxide (DMSO) at a wavelength of 264 nm. It is worth mentioning that PLGA does not interfere with the ibuprofen absorbance at this wavelength.

The drug loading and encapsulation efficiency were calculated as follows:

$$Theoretical\ drug\ loding, TDL\ (\%) = \frac{drug\ used\ for\ encapsulation}{drug + polymer}$$

$$Loading\ efficiency, LE\ (\%) = \frac{encapsulated\ drug}{nanoparticle\ weigth}$$

$$Encapsulation\ efficiency, EE\ (\%) = \frac{LE}{TDL}$$

All dissolution tests were measured by means of UV-Visible spectrophotometer (Agilent Technology, Cary 60). The NPs suspensions were placed in a dialysis bag by suspending a weighed amount of sample in phosphate buffered saline (PBS, pH 7.4). The samples were incubated at 37 °C under magnetic stirring at 100 rpm for 120 h. At specific intervals, 2 ml of sample was withdrawn from the PBS bath and replenished with 2 ml of fresh PBS. The amount of ibuprofen was measured at a wavelength of 264 nm. The experiments were repeated three times.

2.7. Characterization

Dynamic Light Scattering

All NPs and nanocluster suspensions were analysed using the 3D LS spectrometer (LS instruments) to measure their particle size distribution. Approximately 1 ml of the suspension was pipetted into a glass tube without further dilution. DLS measurements were performed in autocorrelation mode with single illuminating beam and single detector. The hydrodynamic radius is calculated by the software of the 3D LS Spectrometer. Three measurement of 30 s duration were repeated, all made at a scattering angle of 90° at room temperature.

Zetasizer potential

The zeta potential of the NPs in the suspensions was analysed by means of Zetasizer Nano ZS (Malvern Instruments) using the Smoluchowski model. Around 800 µl was pipetted from the suspension diluted ten times the initial volume into the cuvette and measured at room temperature. All measurements were performed at room temperature with deionised water as the media. Three runs were performed for each measurement.

Static Light Scattering

Size of the microclusters was analysed using static light scattering technique (Malvern, Mastersizer 2000). The suspensions were diluted ten times the initial volume and injected into the system at a constant rate. The measured intensity of the scattered light, $I(q)$, was used to evaluate the mean radius of gyration $\langle R_g \rangle$ of prepared clusters. For more details, please see supporting information.

Scanning Electron Microscopy

Scanning Electron Microscopy (SEM) was used to analyse the morphology of the NPs. Prior to measurement, for a proper visualization of the NPs, an aliquot of the primary PLGA suspension was freeze dried. Then, the freeze-dried powder was coated with a thin layer (5 nm) of gold and was analysed by electron microscope Mira 3 LMH (Tescan Brno, s.r.o.) equipped with Shottky cathode.

Transmission Electron Microscopy

Visualization of IO NPs and clusters was performed by Transmission Electron Microscopy by 100 kV TEM, model JEM-1010 (JEOL, Ltd) equipped with CCD camera MegaView III (Olympus Soft Imaging Systems, Germany). 10 µl of the sample was deposited on a carbon coated electron microscopic grid, followed by contrasting of the sample by ethanol solution of 1% uranyl acetate. The grid was left for a few minutes to dry and subsequently was inserted into the electron microscope column for the sample analysis. Measurements were performed under 80 kV of accelerating voltage.

X-ray diffraction

X-ray diffraction (XRD) was utilized to characterize the solid-state properties of IO NPs. It was performed with a θ-θ powder diffractometer X'Pert3Powder in Bragg-Brentano para-focusing geometry using wavelength CuK∝ radiation. Data were obtained using an ultrafast detector 1D PIXcel angular range 5-50° (2θ). Data were evaluated using HighScorePlus 4.0.

Fourier transform infrared spectroscopy

The chemical structure of the produced NPs was characterized using Thermo Scientific Nicolet Nexus 670 FTIR spectrometer spectroscopy in transmission mode. Pellets containing the freeze-dried NPs to be analysed were prepared using KBr. 128 scans were collected for each spectrum with resolution of 4 cm^{-1}.

Nuclear magnetic resonance

^{1}H-NMR analysis were performed on a Bruker Avance III 500-MHz spectrometer. Deuterated chloroform ($CDCl_3$) was used as solvent and tetramethylsilane (TMS) as an internal reference. The ^{1}H NMR spectra were used to determine the ratio of the monomers in the analysed copolymers.

Size Exclusion Chromatography

The evolution of the mass average molar mass, Mw, and dispersity, Đ, of PLGA NPs during the dissolution tests was followed using an integrated SEC system from Waters (Milford, MA, USA) equipped with a differential refractive index detector. The molar mass distributions of the samples were analyzed using two PSS Lux LIN M columns (7.8 mm × 300 mm) at 35 °C in THF at an elution rate of 1 mL·min^{-1}. M_w values were calculated in Waters Breeze 3.30 software based on narrow polystyrene (PS) standards (580-1,200,000 g·mol^{-1}).

Vibrating sample magnetometer

The magnetic properties of prepared nanocomposite samples were examined by using a vibrating sample magnetometer (VSM 7407, Lake Shore, USA) in the presence of the applied magnetic field from -10 kOe to +10 kOe at room temperature.

Thermogravimetric Analysis (TGA)

Thermogravimetric analyses (TGA) were performed in Stanton-Redcroft TG 750 under air atmosphere (20 ml·min^{-1}) from room temperature to 700 °C at a rate of 10 °C min^{-1}.

3. Results and discussion

3.1. Mean size, morphology and surface properties of the primary nanoparticles

PLGA was synthesized by bulk ring opening (co)polymerization (ROP) of L-lactide and glycolide initiated with butane-1,4-diol and catalysed with tin(II) ethylhexanoate. After optimization of the variables such as the proportion of the tin(II) ethylhexanoate catalyst and butane-1,4-diol as coinitiator, the targeted low molecular weight PLGA characterized by Mw = 10 kg/mol and molar ratio D,L-lactide/glycolide of 67/33, according to SEC and ^{1}H-NMR (**Figure S1 and Figure S2**) was obtained. To avoid agglomeration of the NPs, repulsive (Coulombic) and attractive forces (Van der Walls) present in the colloidal system must reach the thermodynamic equilibrium. This

concept has already been studied based on the DLVO theory, where as a rule of thumb, absolute values in zeta potential of about ±30 mV provide long term system stability [32]. This is important since long-term storage of the suspensions is essential for a desirable system. PLGA is widely used as a drug delivery vehicle because of its biocompatibility, sustained drug release and biodegradability [33]. By applying different types of coatings, i.e. negatively, positively charged or neutral it becomes possible to tune the properties of the NP surface for a particular target [34, 35]. In this regard, PLGA NPs coated with PEI or with ALG, were prepared by nanoprecipitation method following the biomedical recommendations [31–34]. Indeed, PEI has unique properties as it is highly branched liquid water soluble polyamine with high cationic charge density and it has a broad buffer capacity over a wide range of pH [36]. ALG on the other hand, which is a biodegradable polymer, used as a stabilizer for emulsions, binder or suspending agent, contains a high negative charge density [37]. pH values of the primary particle suspensions are summarized in **Table 3**. The average particle diameter and zeta potential of the primary PLGA NPs obtained by DLS are summarized in **Table 3**. They were measured at pH 6.5 (suspensions diluted ten times the initial volume with deionised water). As can be seen, particles prepared with either PEI or ALG coating have comparable size with diameter in the range of 205 – 225 ± 50 nm as measured by DLS. The morphological observations made by SEM analysis of the PLGA NPs shown in **Figure 1A**, indicate the spherical form of the particles, with particle size equivalent to that obtained by DLS. Zeta potential values, which are for PLGA-PEI 0.05% about 61 ± 8 mV and for PLGA-ALG 1% – 75 ± 8 mV, confirm the high colloidal stability of the prepared NPs. Size and zeta potential distribution of the primary nanoparticles is shown in **Figure S3 and S4.** Increasing the amount of PEI to 0.2 % did not lead to statistically significant change in zeta potential. This indicates that PEI as well as ALG adsorb at the surface of PLGA NPs and act as efficient stabilizers, forming a

stable coating layer regardless the repeated washings for purification [38]. Interestingly enough, ibuprofen loaded PLGA NPs (PLGA-PEI 0.05%_Ibu) exhibited much lower value of Zeta potential about 15 ± 4 mV, when 0.05 wt.% PEI aqueous solution is used during the nanoprecipitation step. This discrepancy could be explained by the presence of acid groups of ibuprofen close to the periphery of PLGA NPs, which may create hydrogen-bonding interactions with the amine of PEI, hence leading to the decrease of the overall zeta potential of the NPs [39]. Therefore, the concentration of PEI was adjusted to 0.2 wt. % to attain zeta potential values comparable to that of pristine PLGA-PEI 0.05%, i.e. 61 ± 8 mV.

IO NPs surface coated with PAA (IO-PAA) produced by co-precipitation are characterized by a narrow PSD with an average hydrodynamic diameter of about 20 ± 3 nm and a zeta potential of -38 ± 5 mV, according to DLS analysis. TEM image of IO-PAA depicted in **Figure 1B** shows that they exhibit spherical morphology, with an average diameter size around 15 nm, which is in agreement with DLS measurements. ALG and CHIT coated IO NPs displayed a diameter of 81 ± 12 nm and 123 ± 30 nm, respectively, followed by their aggregation shortly after their preparation, which attests for their lack of colloidal stability. Stability of the ALG and CHIT coated NPs is presented in **Figure S5**.

DLS and TEM analysis indicate that the adsorption of sufficient amount of PAA at the surface of IO NPs allowed preventing their agglomeration and introduced a high ionic charge density to the NPs, necessary to construct these heteroclusters via electrostatic interactions of oppositely charged NPs. To identify the physical structure of the IO-PAA NPs, XRD analysis was carried out. XRD pattern of IO-PAA depicted in **Figure S6 and Table S1** indicates the presence of six distinct peaks at $2\theta = 30.1°$, 35.5°, 43.2°, 53.5°, 57° and 62.6°, corresponding to the superparamagnetic magnetite form, i.e. Fe_3O_4, which is consistent with the synthesis conditions [40].

Table 3: Average particle diameter, zeta potential of the primary NPs and pH of the freshly prepared suspensions

	Mean diameter (nm)	Zeta potential (mV)	pH*
PLGA-PEI 0.05%	205 ± 33	61 ± 8	3.2
PLGA-PEI 0.2%	207 ± 32	57 ± 7	3.2
PLGA-ALG 1%	220 ± 23	-75 ± 8	3.0
PLGA-PEI 0.05%_Ibu	205 ± 33	15 ± 4	4.0
PLGA-PEI 0.2%_Ibu	215 ± 42	57 ± 6	3.2
IO-PAA	20 ± 3	-38 ± 5	3.2
IO-CHIT	123 ± 30	55 ± 20	3.0

* pH of the freshly prepared suspensions

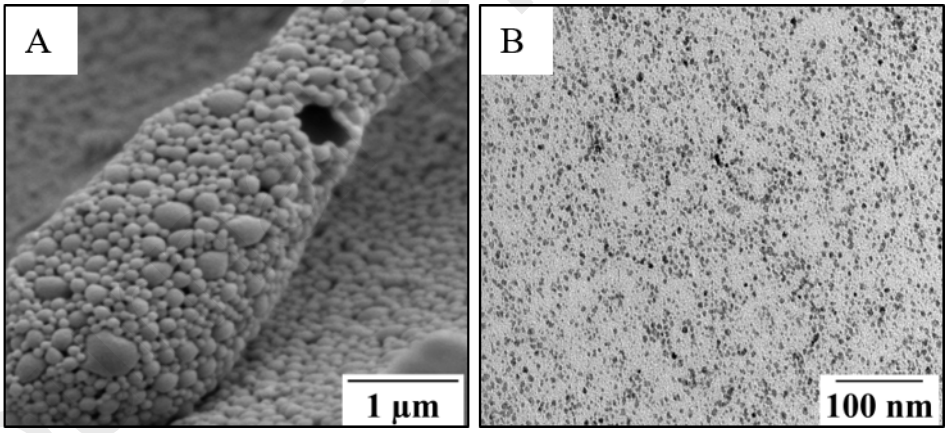

Figure 1: A) SEM picture of PLGA-PEI NPs, B) TEM picture of IO-PAA NPs.

3.2. Clusters formation by self-assembly via electrostatic interactions

Assembly of NPs is dictated by the competition between different inter-particle interactions like electrostatic, Van der Waals, and magnetic interactions, which in turn depends on the material features of the NPs, pH, temperature, dielectric constant of solvent, and existence of external

stimuli [41]. Among these numerous inter-particle interactions, electrostatic interactions are unique, since they are long-ranged, can be repulsive or attractive [42] and can be used for a self-assembly of oppositely charged NPs [43]. Moreover, changing the charge on the NPs and ionic strength enables to tailor their interaction strength and range.

Assembly of NPs is classified into homo-assembly and hetero-assembly, leading to formation of homoclusters, composed of particles of the same chemical composition and heteroclusters, composed of particles of different kind. Hetero-assembly is more complex as NPs with different physical and chemical properties aggregate and is hence not well understood [44].

Since the size of PLGA NPs and IO NPs is significantly different, we investigated impact of NPs size and NPs composition on the properties of formed clusters. Therefore, both homo-assembly as well as hetero-assembly were prepared by self-assembly between the oppositely charged NPs to form clusters via electrostatic interactions either by polymer-polymer NPs (homoclusters) or polymer-inorganic NPs (heteroclusters), following these two methods.

The assembly of the homoclusters involved the primary PLGA NPs with oppositely charged surfaces, i.e. positively charged PLGA-PEI 0.05% characterized by an average diameter of 205 ± 33 nm and Zeta potential of 61 ± 8 mV, and negatively charged PLGA-ALG 1% characterized by an average diameter of 220 ± 23 nm and Zeta potential of -75 ± 8 mV. Formation of the homoclusters was achieved via two approaches, i.e. one-shot versus dropwise addition of one suspension into another in order to examine the effect of the flowrate on clusters formation and on their size. **Figure 2 A** represents the evolution of the average gyration radius, $\langle R_g \rangle$, of the formed clusters as a function of the ratio between PLGA-PEI and PLGA-ALG, following one-shot and dropwise approaches, respectively. Immediately after mixing the suspensions, assembly of the NPs led to the formation of large aggregates with a size in the micrometer range, reaching up to

hundreds of microns according to SLS measurements (**Figure 2**), regardless the approach followed (i.e. one-shot and dropwise). The micro-size of the homoclusters could be attributed to a high ionic strength in the medium, which plays a crucial role on the particle-particle interactions [45]. Nevertheless, the size of these micro-clusters can vary considerably, depending on the processing conditions as can be seen in **Figure 2**. In fact, by varying the ratio PLGA-ALG:PLGA-PEI from 1:1 to 1:4, upon a one-shot approach, a decrease of the size of the clusters from about 100 to 45 μm was measured. When increasing the concentration difference between the oppositely charged NPs suspensions, i.e. ratio PLGA-ALG: PLGA-PEI = 1:6, 1:8 and 1:10, no further size reduction of the clusters can be observed as they remained at around 45 μm. It is worth mentioning that the addition of surfactant such as Tween 80 or implementation of ultrasonication has no impact on their size.

Based on the experimental results, the large size of the homoclusters correlates with the hydrodynamic radius of the NPs and the surface coatings, where the positively charged NPs interact with the negatively charged one. The branched PEI might be the cause of the large size of the clusters, since the NPs possess a high surface charge. Once a large cluster is formed, the size tends to increase due to the strong electrostatic interactions that leads other surrounding NPs to stick together [39]. Therefore, even at smaller concentrations of PLGA-ALG suspension (PLGA-ALG: PLGA-PEI = 1:10), the size of the clusters is still in the micron range. Interestingly enough, as can be seen in **Figure S7,** the size of the homoclusters remained unchanged after 15-day storage period in cold environment (about 8 °C). The stability of the size of the homoclusters overtime suggests that each homocluster reached an optimum equilibrium size which is governed by the ionic strength in the medium. To test the effect of the methodology on the formation of clusters, slow addition with a controlled flow rate of the primary particles was used, considering

only the ratio of 1:1. For a more controlled addition of the NPs suspensions, syringe pumps were used and operated in the range of flow rates between 0.5 to 3.5 mL/min. Examples of such measurements are shown in **Figure 2 B** for PLGA-ALG:PLGA-PEI = 1:1 system. In all cases, the final size of the produced clusters is still in the micron range as the one obtained from PLGA-ALG:PLGA-PEI = 1:1, by one-shot approach. Nonetheless, a decrease in their size was observed when the dropwise approach was used. This trend indicates that the size of the homoclusters, prepared from primary particles with comparable mean size, can be reduced using the dropwise approach (i.e. from 120 ± 8 to 81 ± 4 μm when following one-shot and dropwise approaches, respectively) as a better control of the flow rate of the suspensions during the aggregation step can be achieved. Nevertheless, it did not have a considerable impact on the final size of the homoclusters since they remained in the micron range. The size of the homoclusters at different flow rates remained fairly the same. These results indicate that the size of the homoclusters is governed by the size and strength of interaction between the primary particles, which in turn, is correlated with the nature of the coating agent, i.e. charge and ionic strength, and with the ratio between the oppositely charged particles. Thus, homo-assembly (induced by self-assembly between the oppositely charged NPs via electrostatic interactions) lead inevitably to the formation of large clusters with a size in the micrometer range.

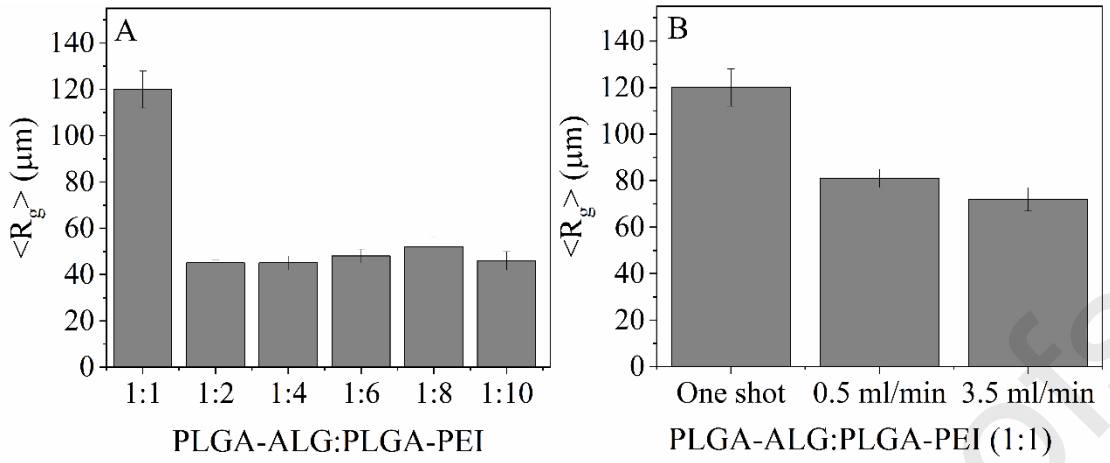

Figure 2: Evolution of the average gyration radius, $\langle R_g \rangle$, of the formed clusters as a function of A) the ratio PLGA-ALG:PLGA-PEI (prepared by one-shot approach), and B) the flow rate (dropwise addition versus one-shot approach) at constant ratio PLGA-ALG:PLGA-PEI (1:1).

Extension of the procedure discussed above for clusters starting from a suspension of all identical primary NPs with the same size, also referred to as homoclusters, to the case where two suspensions composed of two different primary particles with different sizes were carried out. With this respect, to investigate the formation of the heteroclusters via self-assembly of IO and PLGA NPs, different types of positively and negatively charged coatings were applied on their surface, i.e. PAA, CHIT and ALG. Following the same strategy reported for homoclusters, the production of heteroclusters was attained by one-shot and by dropwise approaches. The effect of all involved operating parameters, i.e. ratio (mass) polymer/IO NPs, surfactant type and applied hydrodynamic stress on the size of the heteroclusters was examined. First, it is important to emphasize that after mixing PLGA-ALG and IO-CHIT heteroclusters were formed by the strong interactions of two polysaccharides and the coating concentration. Tested ratios of PLGA-ALG:IO-CHIT= 1:1 and 1:10 reached sizes in the micrometer range (28 and 11 µm respectively), found in **Figure S8** . These oppositely charged NPs are tightly linked together by the inter-particle

attractions and repulsions that can start the formation of a larger network [46]. The reached size for the PLGA-ALG:IO-CHIT heteroclusters is still in the micrometer range, which indicates that the size of the primary particles has an effect on the final result. Therefore, the formation of heteroclusters with primary NPs with even smaller size was investigated following the same strategy, i.e. positively charged PLGA-PEI 0.05% with an average diameter of 205 ± 33 nm and Zeta potential of 61 ± 8 mV, and negatively charged IO-PAA with an average diameter of 20 ± 3 nm and Zeta potential of -38 ± 5 mV. As depicted in **Figure 3A and 3B**, the size of the heteroclusters produced by self-assembly of IO-PAA and PLGA-PEI NPs via one-shot approach is dependent on the ratio IO-PAA:PLGA-PEI. In particular, for the ratios ranging from 1:1 to 1:3, heteroclusters with the sizes ranging from 55 to 25 μm, were obtained, respectively. When the concentration of IO NPs is lower (i.e. ratio IO-PAA:PLGA-PEI equal to 1:3.25), the size of the heteroclusters is in the nanometer range. Further decrease of the concentration of IO-PAA, i.e. ratio IO-PAA:PLGA-PEI ranging from 1:3.25 to 1:100, leads to a significant decrease of the size of the heteroclusters, with sizes in the range of nanometers, from 330 nm for 1:3.25 to 203 nm for 1:100. TEM pictures of the heteroclusters shown in **Figure 4** confirmed this trend. It is worth noting that all heteroclusters prepared by one-shot approach exhibited a positive Zeta potential, which increases with the decrease of IO-PAA concentration, e.g. 27 and 50 mV in the case of heteroclusters prepared from the ratios IO-PAA:PLGA-PEI 1:3.25 and 1:100, respectively. This positive Zeta potential is due to the presence of amine groups from PEI used to coat PLGA NPs. It indicates that IO-PAA NPs locate preferentially between PLGA-PEI NPs, thus playing a role of a binder for the latter via strong electrostatic interactions, due to their smaller average hydrodynamic diameter of 20 nm compared to PLGA-PEI. This explains on one hand the positive Zeta-potential recorded at low IO-PAA concentrations, and on the other hand the formation of

microstructures at higher IO-PAA content, i.e. ratios IO-PAA:PLGA-PEI ranging from 1:1 to 1:3. This behaviour is confirmed by TEM analysis where the distribution of IO-PAA NPs around PLGA-PEI is heterogeneous. The surface coverage of PLGA-PEI with IO-PAA decreases with the decrease of the concentration of the latter, which correlates with the evolution of the Zeta potential values. Decrease of IO-PAA NPs concentration leads to fewer particles assembling around the polymeric NPs compared to the higher ratio. Using the one-shot approach, no careful control over the size of the heteroclusters was reached and no change in the zeta potential was observed.

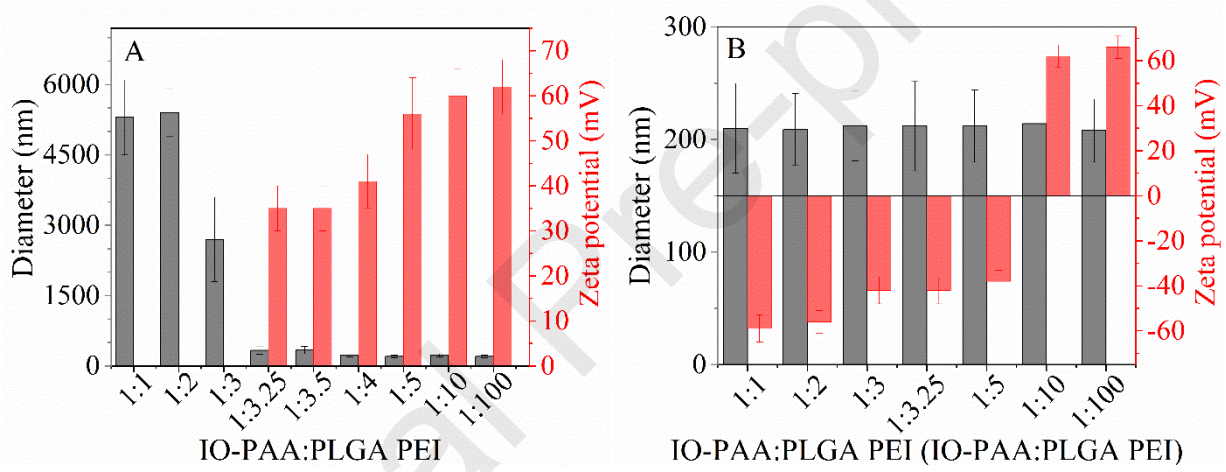

Figure 3: Mean size and Zeta potential of heteroclusters of IO-PAA:PLGA-PEI. Based on one-shot addition of IO NPs into polymeric NPs (A) and mixture of each suspension by slow addition using flow rate of 0.5 ml/min where concentration of polymeric NPs was kept constant (B).

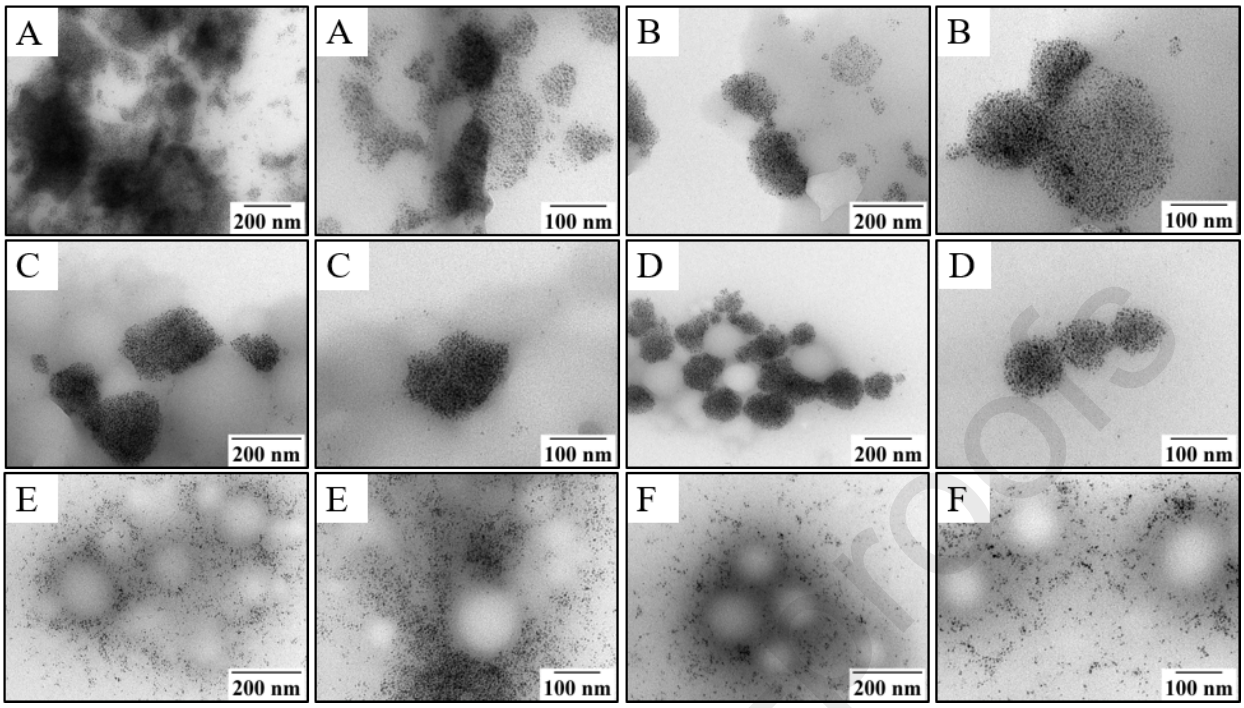

Figure 4. TEM pictures of heteroclusters produced by one-shot approach from the ratios IO-PAA: PLGA-PEI. Ratios A) 1:1; B) 1:2; C) 1:3; D) 1:3.25; E) 1:5 and F) 1:10.

For a sake of better control of the size of the heteroclusters, a dropwise approach, which allows a control of the flow rate, was also employed in this case. Similarly to the homoclusters, the evolution of the size and zeta potential of the heteroclusters as a function of the ratio IO-PAA:PLGA-PEI was thoroughly investigated and the obtained results are depicted in **Figure 3B**. At a constant flow rate of 0.5 ml/min of both IO-PAA and PLGA-PEI suspensions, and a constant mixing speed, clusters with a nanometer size of about 200 ± 26 nm were produced regardless the ratio between the polymeric and inorganic NPs. The formation of the heteroclusters is confirmed by the negative values of the zeta potential of about -48 ± 6 mV, which corresponds to that of IO-PAA in the clusters where sufficient amount of IO-PAA NPs is present in the mixture. Indeed, at relatively low IO-PAA NPs, i.e. ratios of IO-PAA:PLGA-PEI above 1:10, the Zeta-potential

values become positive. It is important to emphasize that the size and the Zeta potential of the clusters are not affected by the increase or the decrease of the flow rates (e.g. 0.25 and 1 ml/min) as can be seen in **Figure S9**. These results reveal that in this case the heteroclusters are formed via a mechanism of adsorption of IO-PAA NPs, on the surface of PLGA-PEI NPs during the slow dropwise process thanks to the establishment of inter-particle electrostatic interactions, hence leading to the formation of nanostructures. In presence of sufficient amount of IO-PAA, a complete coverage of the surface of PLGA-PEI can be achieved. **Figure 5** gathers the representative morphologies of the clusters at nano-scale level (TEM images), where it can be clearly observed that IO-PAA NPs cover the surface of PLGA-PEI NPs, thus confirming the above proposed mechanism of cluster formation. The degree of coverage depends on the ratio between the oppositely charged NPs. These results allow drawing some conclusions about the conditions of cluster's formation by dropwise approach in terms of i) size of the oppositely charged particles where the hydrodynamic diameter of IO-PAA is at least ten times smaller than that of PLGA-PEI, ii) charge and ionic strength of the NPs provided by the coating agent, iii) the ratio between the oppositely charged particles [45], and iv) better control of the assembly kinetics, and therefore statistical distribution of IO-PAA on the surface of PLGA-PEI via dropwise addition of the suspensions. The evolution of size of the heteroclusters prepared by both one-shot and dropwise addition approaches and stored in cold environment (about 8 °C in the fridge) overtime was also examined (**Figure S10**). **Figure S10 A and B** indicate that the size of the heteroclusters did not change after 15-day storage period regardless the methodology applied for their preparation. Accordingly, as in the case of the homoclusters, an optimum size was reached for each heterocluster during their preparation. As aforementioned, this size is associated with the size of the primary NPs and the ionic strength in the medium.

It is worth mentioning that while all IO NPs are attracted by the permanent magnet and, thus, accumulate on the wall of the vial in the direction of the magnetic field **(Figure 6),** the PLGA NPs and their corresponding homoclusters do not display any sensitivity towards the magnetic field. The sedimentation of the homoclusters is only due to the gravitational field **(Figure 6)**. However, the heteroclusters IO-PAA:PLGA-PEI are sensitive to the magnetic field as they sediment under its stimulus **(Figure 6)**. In addition, the visual observation of all formed heteroclusters indicates that they exhibit light brown colour, suggesting a good homogenization between individual dark IO-PAA and white PLGA-PEI NPs. Similar behaviour was found also previously when combining polymeric and IO NPs considering only aggregation mechanism, supporting generality of the assembly process [47].

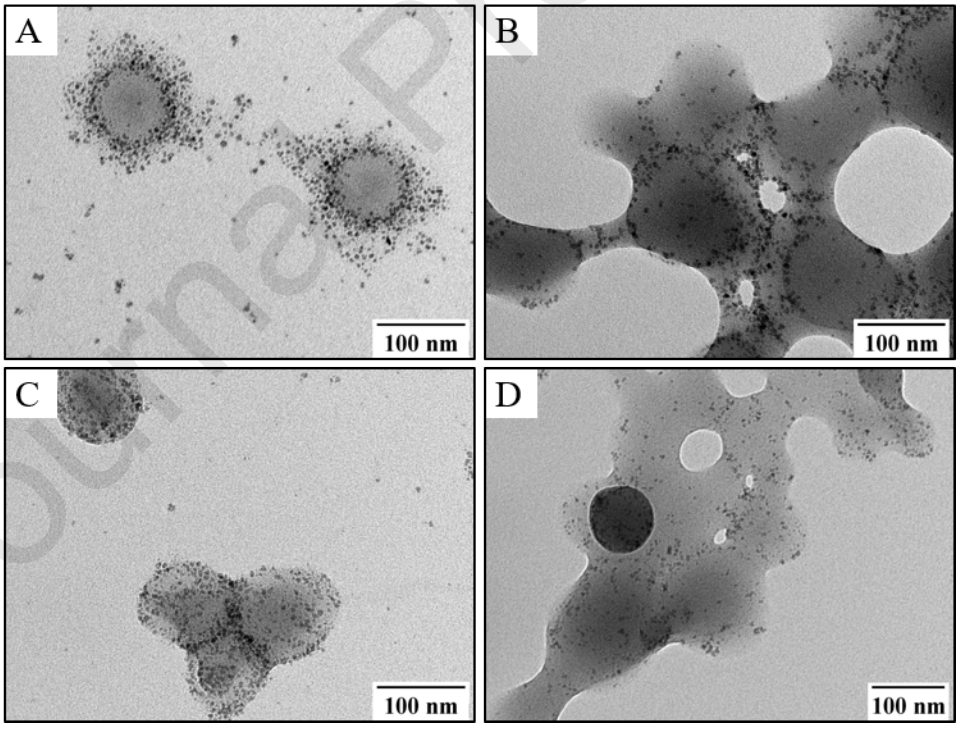

Figure 5. TEM images of heteroclusters produced by dropwise approach with 0.5 ml/min flow rate from the ratios IO-PAA: PLGA-PEI. A) 1:1; B) 1:3; C) 1:3.25 and D) 1:5.

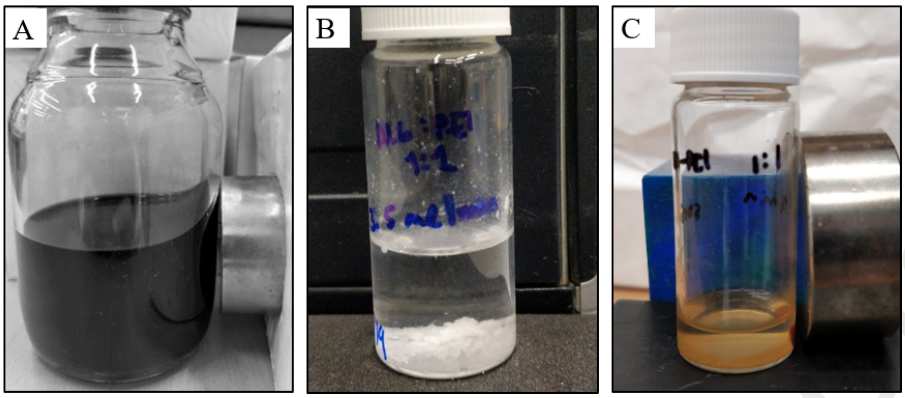

Figure 6. Visual magnetic properties of IO-PAA NPs (A); visual observation of the sedimentation of the homoclusters PLGA-PEI:PLGA-ALG for a ratio of 1:1 (B) and visual magnetic properties of the heteroclusters IO-PAA:PLGA-PEI for ratio of 1:1 (C).

4. Production of drug loaded heteroclusters and their dissolution testing

In order to reach the main goal of the study and develop procedure for preparation of heteroclusters for controlled drug delivery systems, the above described hetero-assembly process using a dropwise approach was applied using oppositely charged ibuprofen loaded PLGA-PEI NPs (PLGA-PEI 0.2%_Ibu) and IO-PAA NPs.

Based on the size and Zeta potential of the primary NPs, i.e. PLGA-PEI 0.2_Ibu and IO-PAA, shown in **Table 3**, the assembly of the heteroclusters is expected to occur. Encapsulation of a model drug, i.e. ibuprofen, was carried out by nanoprecipitation method with an encapsulation efficiency of about 30 ± 5%., followed by the preparation of the heterocluster. Calibration curves of ibuprofen determining the encapsulation efficiency and drug release is depicted in **Figure S11.** For illustration, heteroclusters made of PLGA-PEI 0.2%_Ibu and IO-PAA in a ratio 1:3 were prepared with a controlled flow rate of 0.5 ml/min, thus producing heteroclusters with a nanometer size of about 224 ± 52 nm. The formation of these heteroclusters was evidenced by the change in

the Zeta potential from positive to negative values of about -51 ± 6 mV, as a result of the adsorption of IO-PAA on the surface of PLGA-PEI 0.2%_Ibu. These findings were confirmed by TEM pictures of the heteroclusters shown in **Figure 7**, where it is possible to distinguish between PLGA-PEI 0.2%_Ibu spherical NPs and the much smaller IO-PAA NPs, which are covering the surface of the former.

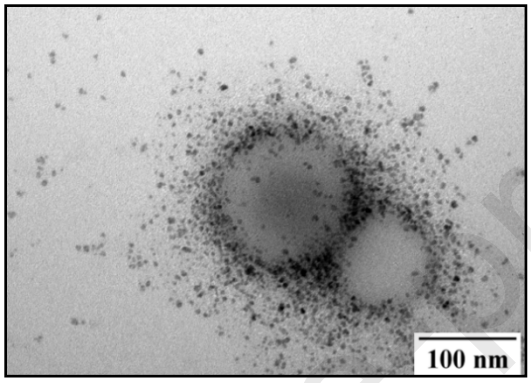

Figure 7. TEM image of heteroclusters formation with encapsulated drug. IO-PAA:PLGA-PEI 0.2%_Ibu with ratio 1:3 using slow addition.

The performance of the heteroclusters as a drug delivery carrier was examined by evaluating their dissolution release profiles in comparison with ibuprofen loaded PLGA NPs. Release profiles of PLGA-PEI 0.2%_Ibu (PLGA NPs) and IO-PAA:PLGA-PEI 0.2%_Ibu (heteroclusters) depicted in **Figure 8** showed an initial burst release phase after 3h, that typically involves hydration of drug molecules on the surface, formation of cracks on the matrix or disintegration of particles [48]. Dissolution profiles indicate also that the release rate of ibuprofen loaded PLGA NPs became slower than that of the heteroclusters after 24 h of dissolution test. In fact, the drug release from the heteroclusters becomes faster after 24 h, leading to a cumulative drug release of about 85 ± 3% at 120 h, while for the PLGA NPs it reached 74 ± 2%.

Further analysis of PLGA-PEI 0.2%_Ibu and IO-PAA:PLGA-PEI 0.2%_Ibu before and after dissolutions tests was carried out for a complete understanding of the drug release mechanism by means of SEC, TGA and FTIR.

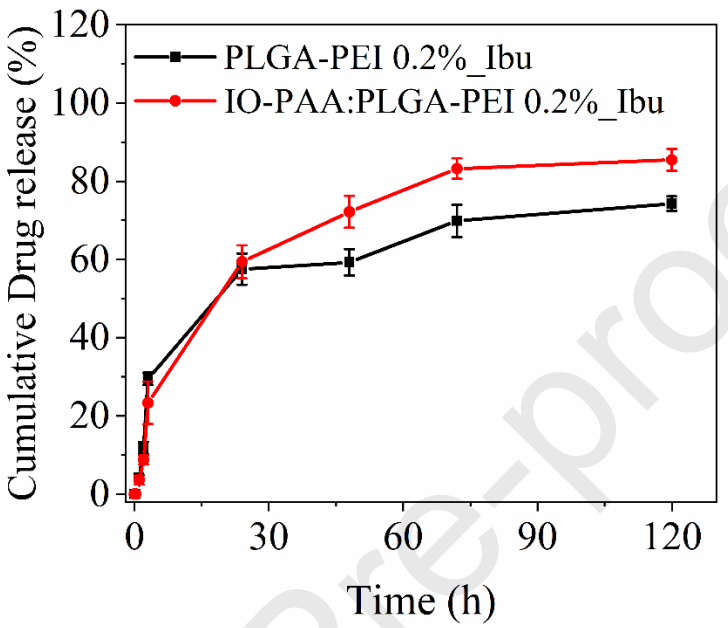

Figure 8. Drug release profiles of PLGA-PEI 0.2%_Ibu NPs and IO-PAA:PLGA-PEI 0.2%_Ibu heteroclusters over the course of 120 h in PBS at 37 °C, pH 7.4.

PLGA, as other biodegradable polyesters, is sensitive to degradation by hydrolysis. Therefore, SEC analysis were carried out to estimate the apparent molar mass (Mn) of PLGA in both PLGA-PEI 0.2%_Ibu and IO-PAA:PLGA-PEI 0.2%_Ibu before and after dissolution tests.

The results obtained by SEC, summarized in **Table 4,** indicate a similar dispersity index (Đ) and molar mass (M_n) of PLGA-PEI 0.2%_Ibu and IO-PAA:PLGA-PEI 0.2%_Ibu before dissolution tests. However, after dissolution tests, the heteroclusters as well as PLGA NPs became insoluble in the eluent. This suggests that PLGA matrix underwent degradation process by hydrolysis leading to the formation of insoluble byproducts in both heteroclusters as well as PLGA NPs.

Table 4. SEC analysis results for the clusters and ibuprofen loaded NPs

Material	M_n (kg/mol)	Đ	M_p (kg/mol)[a]	Note
PLGA-PEI 0.2%_ Ibu_before dissolution tests	8.2	1.7	13.0	
PLGA-PEI 0.2%_Ibu_after dissolution tests	-	-	-	95% insoluble
IO-PAA:PLGA-PEI 0.2%_Ibu_before dissolution tests	9.0	1.5	13.0	
IO-PAA:PLGA-PEI 0.2%_Ibu_after dissolution tests	-	-	-	95% insoluble

[a] molar mass value at peak maximum

For a better understanding of the degradation mechanism of PLGA in both PLGA NPs and heteroclusters, TGA analysis were carried on the latter materials before and after dissolution tests. The TGA curves for PLGA-PEI 0.2%_Ibu and IO-PAA:PLGA-PEI 0.2%_Ibu before and after dissolution tests are depicted in **Figure 9**, and those related to the reference materials, i.e. neat PLGA, PAA and IO-PAA NPs are shown in **Figure S12.** The TG curve corresponding to neat PLGA exhibits one weight loss stage at 390 °C related to its thermal degradation process [25]. The thermal decomposition of both PLGA-PEI 0.2%_Ibu and IO-PAA:PLGA-PEI 0.2%_Ibu began at lower temperatures (208 – 300 °C) compared to neat PLGA. This can be due to the large specific surface area of NPs compared to neat polymer, making them more sensitive to thermal degradation [49]. Interestingly, while PLGA-PEI 0.2%_Ibu NPs showed very similar thermal behavior before and after dissolution tests, a prominent difference between the TG curves of IO-PAA:PLGA-PEI 0.2%_Ibu heteroclusters were observed before and after the drug release tests. The TG curve of IO-PAA:PLGA-PEI 0.2%_Ibu showed a weight loss of 15% from 23 to 220 °C which is attributed to the moisture and residual solvent release, followed by a 75% weight loss corresponding to the thermal decomposition of the polymeric part (coating agents and PLGA) from 220 to 600 °C. After

dissolution tests, the heteroclusters exhibited around 10% weight loss from 23 to 220 °C due to the moisture and residual solvent release, followed by a weight loss of about 10% that occurred from 220 to 600 °C, which correspond to the thermal decomposition of the coating agents and the polymeric fraction (coating agents and remaining PLGA and/or its byproducts formed during the dissolution tests by hydrolysis). The overall degradation of the heteroclusters up to 800 °C reaches a total weight loss of 90 and 20 wt. %, before and after dissolution tests, respectively. This indicates that during the dissolution tests the degradation of PLGA is catalyzed by the presence of IO NPs, which can explain the faster drug release observed after 24 h in the heteroclusters compared to PLGA NPs. It worth indicating that the remaining solid content after thermal degradation of the heteroclusters up to 800 °C corresponds to the content of Fe_3O_4 (without coating). Thus, According to TG curves, the content of Fe_3O_4 in IO-PAA:PLGA-PEI 0.2%_Ibu before and after dissolution tests is about 10 and 80 wt.% of the total solid content, respectively.

FTIR analysis carried out on the PLGA NPs and the heteroclusters before and after the dissolution tests did not reveal any chemical changes as can be seen in **Figure S13**, thus indicating that the remaining polymeric part in the heteroclusters after dissolution tests is mainly composed of PLGA and/or its byproducts such as oligomers.

Studies have been reported about the stages of degradation for PLGA based on FTIR, where in the first stage, the mass of glycolic and lactic acid units remain relatively constant for the first week in PBS at pH 7.4. The first stage is dependent on the lactic acid content in the polymer, where for a higher lactic content, there is higher time needed to observe a significant chemical change [50]. Therefore, based on FTIR, PLGA NPs and heteroclusters showed no structural changes on the remaining solid fraction. Nonetheless, based on the results by SEC, it suggests that during the

dissolution, the PLGA underwent a severe degradation process and the release of ibuprofen was accelerated for the heteroclusters, thanks to the catalytic effect of IO NPs.

Finally, the magnetic properties of the formed heteroclusters were envisaged by magnetization curves before and after the dissolution tests. From **Figure 10,** the magnetic properties of the heteroclusters exhibited superparamagnetism without magnetic hysteresis. This indicates that IO NPs did not undergo degradation during the dissolution tests up to 120 h, which is in good agreement with TGA analysis. Hence, even after drug release, the heteroclusters can be used for hyperthermia.

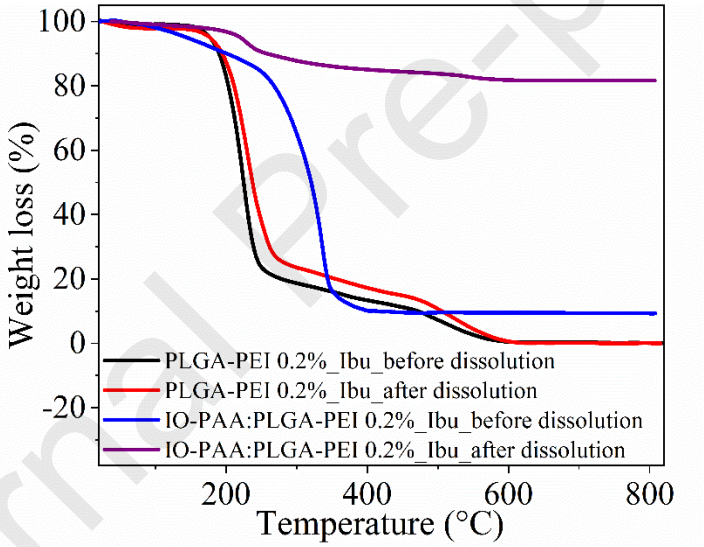

Figure 9. TG curves for PLGA-PEI 0.2%_Ibu and before and IO-PAA: PLGA-PEI 0.2%_Ibu before and after dissolution

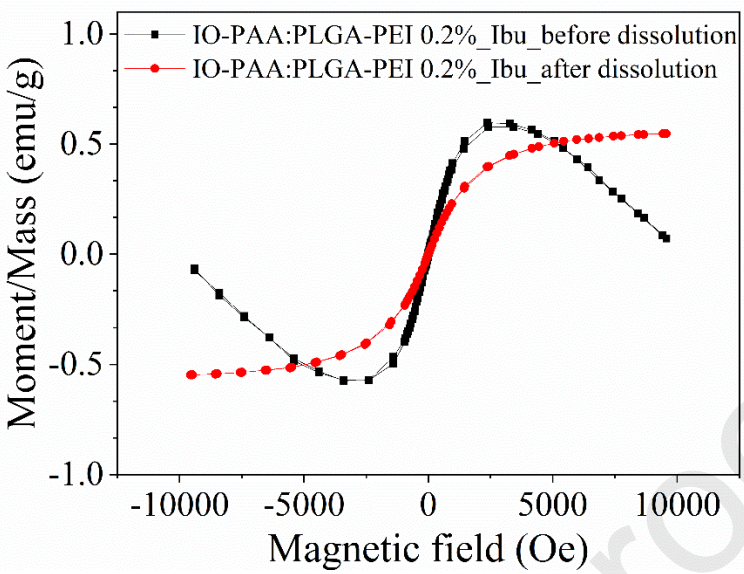

Figure 10. Magnetization curves for IO-PAA:PLGA-PEI 0.2%_Ibu heteroclusters before and after dissolution tests

5. Conclusions

A simple and versatile method based on self-assembly *via* electrostatic interactions of oppositely charged PLGA and IO NPs was developed in order to construct controlled drug delivery nanoclusters. Formation of the clusters was achieved via two approaches, i.e. one-shot versus dropwise addition of one suspension into another. Impact of processing conditions such as nature of the coating, ratio between oppositely charged particles and mixing parameters on the size and stability of prepared clusters was evaluated. The assembly of the homoclusters involved the primary PLGA NPs with oppositely charged surfaces, i.e. positively charged PLGA-PEI 0.05% characterized by an average diameter of 205 ± 33 nm and Zeta potential of 61 ± 8 mV, and negatively charged PLGA-ALG 1% characterized by an average diameter of 220 ± 23 nm and Zeta potential of -75 ± 8 mV. Formation of homoclusters with a size in the micrometer range was obtained. It was observed that the size of the homoclusters, prepared from primary particles with

comparable mean size, is not affected by the methodology applied, as a better control of the flow rate of the suspensions during the aggregation step did not have an impact on the final size of the homoclusters. It is governed by the size and strength of interaction between the primary particles, which in turn is correlated with the nature of the coating agent.

The heteroclusters were obtained by the assembly of positively charged PLGA-PEI 0.05% with an average diameter of 205 ± 33 nm and Zeta potential of 61 ± 8 mV, and negatively charged IO-PAA with an average diameter of 20 ± 3 nm and Zeta potential of -38 ± 5 mV. In contrast with homoclusters formation, the size of the produced heteroclusters were dependent on the processing parameters like the flow rate of the suspensions and the ratio between both types of NPs. In fact, the size of the heteroclusters produced by one-shot approach was dependent on the ratio IO-PAA:PLGA-PEI. In particular, for the ratios ranging from 1:1 to 1:3, heteroclusters with a size in the micrometer range were obtained. When the concentration of IO NPs is lower, the size of the heteroclusters is in the nanometer range. It was found out that using this approach, IO-PAA NPs locate preferentially between PLGA-PEI NPs, thus playing a role of a binder for the latter. Interestingly, the dropwise approach leads to the formation of heteroclusters with a nanometer size of about 200 ± 26 nm, regardless the ratio between the polymeric and inorganic NPs. Using this approach a better control of the cluster size was achieved. In this case the heteroclusters are formed *via* a mechanism of adsorption of IO-PAA NPs on the surface of PLGA-PEI NPs. During this study a better control of the clusters' size was observed by the dropwise approach for both types of clusters. More importantly, the controlled formation of nanoclusters was achieved by employing primary nanoparticles of different size.

The dissolution release performance of the heteroclusters as a drug delivery carrier was examined and compared with that of PLGA-PEI NPs. Dissolution tests demonstrated an accelerated drug

release in the heteroclusters after 24 h. This was correlated with the catalytic effect of IO NPs on the degradation of PLGA matrix. The magnetic properties of the heteroclusters were maintained after the dissolution test, thus indicating that IO NPs did not undergo degradation during the dissolution tests up to 120 h. Hence, even after drug release, the heteroclusters can be used for magnetically mediated hyperthermia.

Consequently, this study is invaluable for understanding the release mechanism of an encapsulated drug for a multicomponent drug delivery system and the parameters that influence the release rate in order to be able to modify and control the desired properties. Further optimization of the final size of the nanoclusters below 100 nm is expected as well as to determine the in-vitro cell cytotoxicity of the prepared clusters.

Acknowledgement:

The authors would like to acknowledge the funding by the grant of Ministry of Health of the Czech Republic (AZV 16-34342A) and the specific university research grant (A2_FCHI_2020_031). Jean-Marie Raquez is a FRS-FNRS research associate. The authors would like to acknowledge Mr. Xavier Carette for assistance in the laboratory and Dr. Rosica Mincheva for the fruitfull discussions.

Data availability

The raw/processed data required to reproduce these findings can be shared at this time upon request.

References

1. Brannon-Peppas, L. and J.O. Blanchette, *Nanoparticle and targeted systems for cancer therapy.* Advanced Drug Delivery Reviews, 2012. **64**: p. 206-212.
2. Schirrmacher, V., *From chemotherapy to biological therapy: A review of novel concepts to reduce the side effects of systemic cancer treatment (Review).* International Journal of Oncology, 2019. **54**: p. 407-419.
3. Torchilin, V.P., *Multifunctional nanocarriers.* Adv Drug Deliv Rev, 2006. **58**(14): p. 1532-55.
4. Ulbrich, K., et al., *Targeted Drug Delivery with Polymers and Magnetic Nanoparticles: Covalent and Noncovalent Approaches, Release Control, and Clinical Studies.* Chemical Reviews, 2016. **116**: p. 5338-5431.
5. Estanqueiro, M., et al., *Nanotechnological carriers for cancer chemotherapy: The state of the art.* Colloids and Surfaces B: Biointerfaces, 2015. **126**: p. 631-648.
6. Brigger, I., C. Dubernet, and P. Couvreur, *Nanoparticles in cancer therapy and diagnosis.* Advanced Drug Delivery Reviews, 2012. **64**: p. 24-36.
7. Danhier, F., O. Feron, and V. Préat, *To exploit the tumor microenvironment : Passive and active tumor targeting of nanocarriers for anti-cancer drug delivery.* Journal of Controlled Release, 2015. **148**: p. 135-146.
8. Parhi, P., C. Mohanty, and S.K. Sahoo, *Nanotechnology-based combinational drug delivery : an emerging approach for cancer therapy.* Drug Discovery Today, 2012. **17**: p. 1044-1052.
9. Baek, S., et al., *Smart multifunctional drug delivery towards anticancer therapy harmonized in mesoporous nanoparticles.* Nanoscale, 2015. **7**: p. 14191-14216.

10. Ye, F., et al., *Biodegradable polymeric vesicles containing magnetic nanoparticles, quantum dots and anticancer drugs for drug delivery and imaging.* Biomaterials, 2014. **35**: p. 3885-3894.

11. Xu, X., et al., *Cancer nanomedicine: From targeted delivery to combination therapy.* Trends in Molecular Medicine, 2015. **21**: p. 223-232.

12. Kim, J., et al., *Designed fabrication of a multifunctional polymer nanomedical platform for simultaneous cancer-targeted imaging and magnetically guided drug delivery.* Advanced Materials, 2008. **20**: p. 478-483.

13. Hu, C.M.J. and L. Zhang, *Nanoparticle-based combination therapy toward overcoming drug resistance in cancer.* Biochemical Pharmacology, 2012. **83**: p. 1104-1111.

14. Sanjai, C., et al., *Chitosan-triphosphate nanoparticles for encapsulation of super-paramagnetic iron oxide as an MRI contrast agent.* Carbohydrate Polymers, 2014. **104**: p. 231-237.

15. Hola, K., et al., *Tailored functionalization of iron oxide nanoparticles for MRI, drug delivery, magnetic separation and immobilization of biosubstances.* Biotechnology advances, 2015. **33**: p. 1162-1176.

16. Laurent, S., et al., *Magnetic fluid hyperthermia: focus on superparamagnetic iron oxide nanoparticles.* Adv Colloid Interface Sci, 2011. **166**(1-2): p. 8-23.

17. Sun, C., J.S.H. Lee, and M. Zhang, *Magnetic nanoparticles in MR imaging and drug delivery.* Advanced Drug Delivery Reviews, 2008. **60**: p. 1252-1265.

18. Veiseh, O., J.W. Gunn, and M. Zhang, *Design and fabrication of magnetic nanoparticles for targeted drug delivery and imaging.* Advanced Drug Delivery Reviews, 2010. **62**: p. 284-304.

19. Mornet, S., et al., *Magnetic nanoparticle design for medical diagnosis and therapy.* Journal of Materials Chemistry, 2004. **14**(14): p. 2161.

20. Lam, P.L., et al., *Recent advances in green nanoparticulate systems for drug delivery: efficient delivery and safety concern.* Nanomedicine (Lond), 2017. **12**(4): p. 357-385.

21. Kostiainen, M.A., et al., *Electrostatic assembly of binary nanoparticle superlattices using protein cages.* Nature Nanotechnology, 2013. **8**: p. 52-56.

22. Dechy-Cabaret, O., B. Martin-Vaca, and D. Bourissou, *Controlled ring-opening polymerization of lactide and glycolide.* Chemical Reviews, 2004. **104**: p. 6147-6176.

23. Fredenberg, S., et al., *The mechanisms of drug release in poly (lactic-co-glycolic acid) - based drug delivery systems — A review.* International Journal of Pharmaceutics, 2011. **415**: p. 34-52.

24. Govender, T., *PLGA nanoparticles prepared by nanoprecipitation: drug loading and release studies of a water soluble drug.* Journal of Controlled Release, 1999. **57**: p. 171-185.

25. D'Avila Carvalho Erbetta, C., *Synthesis and Characterization of Poly(D,L-Lactide-co-Glycolide) Copolymer.* Journal of Biomaterials and Nanobiotechnology, 2012. **03**: p. 208-225.

26. Aragón, D.M., J.E. Rosas, and F. Martínez, *Effect of the ibuprofen solubility in acetone and dichloromethane on its release profiles from PLGA microspheres* Latin American applied research 2014.

27. Jouyban, A., *Handbook of Solubility Data for Pharmaceuticals*. 2009: CRC Press.

28. Kunath, K., et al., *Low-molecular-weight polyethylenimine as a non-viral vector for DNA delivery: comparison of physicochemical properties, transfection efficiency and in vivo*

distribution with high-molecular-weight polyethylenimine. Journal of Controlled Release, 2003. **89**(1): p. 113-125.

29. Bivas-Benita, M., et al., *PLGA-PEI nanoparticles for gene delivery to pulmonary epithelium.* European Journal of Pharmaceutics and Biopharmaceutics, 2004. **58**: p. 1-6.
30. Zhou, J., et al., *Layer by layer chitosan/alginate coatings on poly(lactide-co-glycolide) nanoparticles for antifouling protection and Folic acid binding to achieve selective cell targeting.* Journal of Colloid and Interface Science, 2010. **345**: p. 241-247.
31. Massart, R., *Preparation of aqueous magnetic liquids in alkaline and acidic media.* IEEE Transactions on Magnetics, 1981. **17**: p. 1247-1248.
32. Honary, S. and F. Zahir, *Effect of zeta potential on the properties of nano-drug delivery systems - A review (Part 1).* Tropical Journal of Pharmaceutical Research, 2013. **12**: p. 255-264.
33. Danhier, F., et al., *PLGA-based nanoparticles: An overview of biomedical applications.* Journal of Controlled Release, 2012. **161**: p. 505-522.
34. Gupta, A.K. and M. Gupta, *Synthesis and surface engineering of iron oxide nanoparticles for biomedical applications.* Biomaterials, 2005. **26**: p. 3995-4021.
35. Yu, D., et al., *Influence of surface coating of PLGA particles on the internalization and functions of human endothelial cells.* Biomacromolecules, 2012. **13**: p. 3272-3282.
36. Merdan, T., J. Kopeček, and T. Kissel, *Prospects for cationic polymers in gene and oligonucleotide therapy against cancer.* Advanced Drug Delivery Reviews, 2002. **54**: p. 715-758.
37. Tønnesen, H.H. and J. Karlsen, *Alginate in drug delivery systems.* Drug Development and Industrial Pharmacy, 2002. **28**: p. 621-630.

38. Abdelwahed, W., G. Degobert, and H. Fessi, *A pilot study of freeze drying of poly(epsilon-caprolactone) nanocapsules stabilized by poly(vinyl alcohol): Formulation and process optimization.* International Journal of Pharmaceutics, 2006. **309**(1): p. 178-188.

39. Feng, M. and P. Li, *Amine-containing core-shell nanoparticles as potential drug carriers for intracellular delivery.* J Biomed Mater Res A, 2007. **80**(1): p. 184-93.

40. Maity, D. and D.C. Agrawal, *Synthesis of iron oxide nanoparticles under oxidizing environment and their stabilization in aqueous and non-aqueous media.* Journal of Magnetism and Magnetic Materials, 2007. **308**: p. 46-55.

41. Hans, M. and A. Lowman, *Nanoparticles for Drug Delivery.* Nanomaterials Handbook, 2006.

42. Singh, K., et al., *Effect of size and charge asymmetry on aggregation kinetics of oppositely charged nanoparticles.* Sci Rep, 2019. **9**(1): p. 3762.

43. Kalsin, A.M., et al., *Ionic-like behavior of oppositely charged nanoparticles.* J Am Chem Soc, 2006. **128**(47): p. 15046-7.

44. Hogg, R., T.W. Healy, and D.W. Fuerstenau, *Mutual coagulation of colloidal dispersions.* Transactions of the Faraday Society, 1966. **62**: p. 1638-1651.

45. Lebovka, N.I., *Aggregation of Charged Colloidal Particles*, in *Polyelectrolyte Complexes in the Dispersed and Solid State I: Principles and Theory*, M. Müller, Editor. 2014, Springer Berlin Heidelberg: Berlin, Heidelberg. p. 57-96.

46. Wang, Q., et al., *PLGA-chitosan/PLGA-alginate nanoparticle blends as biodegradable colloidal gels for seeding human umbilical cord mesenchymal stem cells.* J Biomed Mater Res A, 2011. **96**(3): p. 520-7.

47. Codari, F., et al., *Synthesis of hetero-nanoclusters: The case of polymer-magnetite systems.* Langmuir, 2014. **30**: p. 2266-2273.

48. Xu, Y., et al., *Polymer degradation and drug delivery in PLGA-based drug–polymer applications: A review of experiments and theories.* Journal of Biomedical Materials Research - Part B Applied Biomaterials, 2017. **105**: p. 1692-1716.

49. Mainardes, R.M., M.P.D. Gremião, and R.C. Evangelista, *Thermoanalytical study of praziquantel-loaded PLGA nanoparticles.* Revista Brasileira de Ciências Farmacêuticas, 2006. **42**(4): p. 523-530.

50. Vey, E., et al., *Degradation kinetics of poly(lactic-co-glycolic) acid block copolymer cast films in phosphate buffer solution as revealed by infrared and Raman spectroscopies.* Polymer Degradation and Stability, 2011. **96**(10): p. 1882-1889.

Conflict of Interest.

There is no conflict of interest.

CRediT author statement

Alma Lucia Villela Zumaya: Methodology, Validation, Formal analysis, Investigation, Visualization, Writing - Original Draft

Dominik Martynek: Methodology, Validation, Formal analysis, Investigation

Tereza Bautkinová: Methodology, Validation, Formal analysis, Investigation

Miroslav Šoóš: Conceptualization, Methodology, Validation, Formal analysis, Project administration, Writing - Review & Editing, Supervision

Pavel Ulbrich: Investigation, Validation, Formal analysis, Writing - Review & Editing

Jean-Marie Raquez: Co-supervision, Resources, Validation, Writing - Review & Editing

Marcela Dendisová: Investigation, Validation, Formal analysis, Writing - Review & Editing

Jan Merna: Investigation, Validation, Formal analysis, Writing - Review & Editing

Jarmila Vilčáková: Investigation, Formal analysis, Writing - Review & Editing

Dušan Kopecký: Investigation, Formal analysis, Writing - Review & Editing

Fatima Hassouna: Conceptualization, Methodology, Validation, Formal analysis, Supervision, Project administration, Writing - Original Draft

Graphical Abstract.

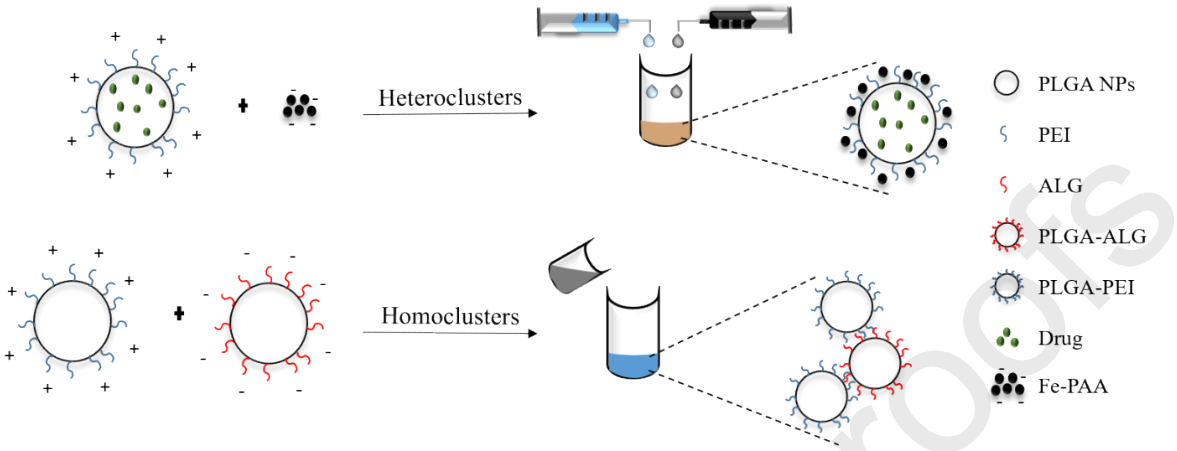

Highlights

- Preparation of a multifunctional controlled drug delivery systems by self-assembly
- Self-assembly of PLGA and magnetic nanoparticles into (nano)clusters
- Effect of the processing parameters on the size and stability of the clusters
- Relationship between the drug release kinetics and clusters properties